Granular Matter 2, 189–199 © Springer-Verlag 2000

Dynamics of deviations from the Gaussian state in a freely cooling homogeneous system of smooth inelastic particles

M. Huthmann, José A. G. Orza, Ricardo Brito

Abstract The time dependence of deviations from the Gaussian state in a freely cooling homogeneous system of smooth inelastically colliding spheres is investigated by kinetic theory. We determine the full time dependence of the coefficients of an expansion around the Gaussian state in Generalized Laguerre polynomials. Approximating this system of equations to sixth order, we find that the asymptotic state, where the mean energy T follows Haff's law with time *independent* cooling rate, is reached within a few collisions per particle. Two-dimensional molecular dynamics simulations confirm our results and show *exponential* behavior in the high-energy tails.

Key words high energy tails, inelastic particles, non-Gaussian behavior, velocity distribution

1 Introduction

Freely cooling systems of smooth inelastically colliding spheres or discs (in the following denoted by inelastic hard spheres systems (IHS)) have been investigated by means of kinetic theory and computer simulations by several groups (see e.g. [1–7]). Most of the studies focus on latest times where interesting phenomena like formation of vortex patterns [5,6] and clustering [1,3,8] can be observed. For short times or not too high inelasticities, however, the system remains homogeneous with a decreasing temperature, or equivalently, a decreasing average velocity. It is the so called Homogeneous Cooling State (HCS) the regime that will be studied in this paper. The HCS admits a *scaling solution*, i.e. if one scales all velocities with the average velocity and assumes that the shape of the scaled velocity distribution function remains constant in time, the entire time dependence is given by the time dependence of the average velocity only. This scaling solution is the starting point for a hydrodynamic analysis. Although many of the existing theories use a Gaussian velocity distribution function (which may be valid for small inelasticity) in general the shape is not Gaussian. First evidence, at very late evolution stages, was obtained by Goldhirsch et al. [2] by measuring the fourth moment of the velocity distribution function. Later Goldshtein and Shapiro [9] proposed a solution based on an expansion in Sonine polynomials. Van Noije and Ernst [10] correctly calculated the first term to linear order and Brilliantov and Pöschel [11] included nonlinear corrections. Numerical solutions of the Boltzmann equation were calculated using Direct Simulation Monte Carlo method (DSMC) [12]. Finally, extensions to viscoelastic particles have been recently presented in [13].

Further confirmation of non Gaussian behavior is given by Esipov and Pöschel [4] by studying the high-velocity tails of the velocity distribution function. They find that the tails are of an exponential type instead of a Gaussian, results confirmed by DSMC by Brey *et al.* [14] and also in experiments performed by Losert and coworkers [15]. In fact, an asymptotic exponential tail of the form $\exp(-v^\beta)$ with $\beta < 2$ seems to be a more fundamental behavior, as it is also present in driven or vibrated granular materials [10,15]. Recently, a detailed study by DSMC in driven systems with three different types of forcing has been presented [16]. Only for the so-called Non-Gaussian thermostat (where there is a balance between energy input and dissipation) $\beta = 2$, while for the other forcings, $\beta = 3/2$ and 1. Surprisingly, no molecular dynamics results have been presented so far for calculating moments and high energy tails for the freely evolving case.

Our starting point is similar to [9], i.e. expand the scaled velocity distribution function in a series of Generalized or Associated Laguerre polynomials around the Gaussian distribution with coefficients denoted with a_l. However, we assume that the coefficients are time dependent [11]. With these ideas we try to achieve two goals. Firstly, investigate the influence of higher coefficients $a_3, \ldots, a_6$, in the expansion of the distribution function. Secondly study their time evolution. We find that for not too high inelasticities the above expansion seems to be convergent. Furthermore, the cooling proceeds in two stages: (1) A fast decay (in the order of few collisions per particle) of all coefficients a_l to their asymptotically constant values. (2) An algebraically slow decay of the kinetic energy T determined by Haff's law $\frac{d}{dt}T = CT^{-3/2}$ and

Received: 10 January 2000

M. Huthmann
Institut für Theoretische Physik, Universität Göttingen, Bunsenstr. 9, 37073 Göttingen, Germany

A. G. Orza, R. Brito (✉)
Dpto. Física Aplicada I, Facultad de Ciencias Físicas, Universidad Complutense, 28040 Madrid, Spain

The authors thank to A. Zippelius, T. Aspelmeier, P. Müller, and A. Santos for useful discussions. M. H. acknowledges financial support by the DFG through SFB 345 (Germany), and J. A. G. O. and R. B. from DGES number PB97-0076 (Spain).

time independent coefficient C depending on the asymptotic values of a_l. Two dimensional event driven molecular dynamics simulations are performed in order to test the theory with good agreement for moderate inelasticity. For higher inelasticity the perturbations expansions seems to fail and in the simulations we were able to observe a transition to an exponential high-energy tail.

The paper is organized as follows: In Sec. 2 we propose the expansion of the velocity distribution in Laguerre polynomials with time dependent coefficients. In Sec. 3 we determine formally the *full* time dependence of the HCS expressed by the time evolution of the coefficients of the expansion. We obtain an infinitely large system of ordinary differential equations, which can only be investigated approximately. This is done in Sec. 4, where a truncation scheme is proposed and analyzed to different orders. In Sec. 5 we compare the analytical theory to results from event-driven simulations and the validity of the perturbation expansion is discussed. Results for the exponential high-energy tail are presented here. We summarize the results in Sec. 6.

2 The system under consideration

We consider a system of N smooth, inelastically colliding spheres with diameter σ confined to a d-dimensional volume V, so that the homogeneous density is given by $n := \frac{N}{V}$. The positions of each sphere are denoted by $\vec{r}_i$ and each particle has a velocity $\vec{v}_i$. The particles interact via a hard-core potential and in each collision (i.e. if $r_{ij} := |\vec{r}_{ij}| := |\vec{r}_i - \vec{r}_j| = \sigma$) the velocities are instantaneously changed by the following collision rules determined by a constant coefficient $e_n \in [0,1]$ of restitution

$$\begin{aligned}\vec{v}_i' &= \vec{v}_i - \frac{1+e_n}{2}(\vec{v}_{ij}\cdot\hat{r}_{ij})\hat{r}_{ij},\\ \vec{v}_j' &= \vec{v}_j + \frac{1+e_n}{2}(\vec{v}_{ij}\cdot\hat{r}_{ij})\hat{r}_{ij}\ ,\end{aligned} \tag{1}$$

where $\vec{v}_{ij} := \vec{v}_i - \vec{v}_j$ and $\hat{r}_{ij} = \vec{r}_{ij}/r_{ij}$. Velocities *after* collision are primed quantities given by velocities *before* collision (unprimed quantities).

The IHS is described statistically by the single particle distribution function $\rho(\vec{r},\vec{v},t)d\vec{r}d\vec{v}$, the (average) number of particles at positions between $\vec{r}$ and $\vec{r}+d\vec{r}$ and with velocities between $\vec{v}$ and $\vec{v}+d\vec{v}$ at time t. As proposed in [9], for a homogeneous inelastic system the distribution function can be expressed by a scaling function as:

$$\rho(\vec{v},t) := n\frac{1}{(v_0(t)\sqrt{\pi})^d}\tilde{\rho}(\vec{c},t)\ , \tag{2}$$

where $\vec{c} = \vec{v}/v_0(t)$ and $v_0(t)$ is the thermal velocity defined as the square root of the second moment of the distribution function:

$$\int d\vec{v}\,\rho(\vec{v},t)\vec{v}^2 = n\frac{d}{2}v_0^2(t)\ . \tag{3}$$

The temperature is then defined as $T(t) := \frac{m}{2}v_0^2(t)$. For elastic systems the distribution function is Gaussian and it is expected that it will remain close to a Gaussian for small inelasticity. Therefore, we expand the scaled distribution function in a series of Generalized or Associated Laguerre polynomials [17] around the Gaussian distribution function. The expansion is carried out in the scaled velocity variable $\vec{c}$ and with *time dependent coefficients* $a_l(t)$ [11]. The general ansatz for the single particle distributions function for the homogeneous cooling then reads

$$\tilde{\rho}(\vec{c},t) := \exp\left(-\vec{c}^{\,2}\right)\sum_{l=0}^{\infty} a_l(t)L_l^{\alpha}\left(\vec{c}^{\,2}\right)\ , \tag{4}$$

where $\alpha = d/2-1$ in d dimensions. In the context of kinetic theory Laguerre polynomials are called Sonine polynomials [18].

The normalization condition for ρ, $\int d\vec{v}\rho = n$, leads to $a_0 = 1$. We express $\vec{v}^2$ by the first and second Laguerre polynomial

$$\vec{v}^{\,2} = -L_1^{\alpha}(\vec{v}^{\,2}) + (\alpha+1)L_0^{\alpha}(\vec{v}^{\,2})\ , \tag{5}$$

and using the orthogonality relations for the Laguerre polynomials we find

$$\int d\vec{v}\,\rho(\vec{v},t)\vec{v}^{\,2} = nv_0^2\left(\frac{d}{2} - \binom{1+\alpha}{1}a_1\right)\ , \tag{6}$$

which implies together with Eq. (3) that $a_1 = 0$ for all times [9–11]. We denoted the binomial coefficients by $\binom{a}{b}$.

Finally, as Laguerre polynomials are orthogonal, the coefficients a_l are given by

$$na_l(t) = \frac{1}{\binom{l+\alpha}{l}}\int d\vec{v}\,\rho(\vec{v},t)L_l^{\alpha}\left(\left(\frac{\vec{v}}{v_0(t)}\right)^2\right)\ . \tag{7}$$

3 The Homogeneous Cooling State

The Boltzmann Equation

We assume that dynamics of the one particle distribution function ρ is given by the Enskog Boltzmann equation, which can be written in d dimensions without external forces as

$$\partial_t\rho(\vec{r},\vec{v}_1,t) + (\vec{v}_1\cdot\nabla_{\vec{r}})\rho(\vec{r},\vec{v}_1,t) = J[\rho,\rho]\ , \tag{8}$$

with collision integral

$$\begin{aligned}J[\rho,\rho] = \sigma^{d-1}\chi\int d\vec{v}_2\int d\hat{\sigma}\Theta(\vec{v}_{12}\cdot\hat{\sigma})(\vec{v}_{12}\cdot\hat{\sigma})\\ \times\left(\frac{b^{-1}}{{e_n}^2}-1\right)(\rho(\vec{r},\vec{v}_1,t)\rho(\vec{r},\vec{v}_2,t))\ .\end{aligned} \tag{9}$$

$\hat{\sigma}$ is the unit vector pointing from particle 2 to particle 1, χ the pair correlation function at contact, and b^{-1} describes 'restituting collisions' by changing velocities in ρ, i.e. $b^{-1}\rho(\vec{r},\vec{v}'',t) = \rho(\vec{r},\vec{v},t)$ in a way that $\vec{v}''$ are the velocities before collision leading to $\vec{v}$ after collision. The operator b describes 'direct collisions' given in Eqs. (1). The inverse operator of b, i.e. b^{-1}, is simply given by substituting e_n by $1/e_n$ in Eqs. (1).

By multiplying the Boltzmann equation Eq. (8) with some function $\psi(\vec{v}_1)$ and integrating over $\vec{v}_1$ one gets

$$\partial_t \int d\vec{v}_1 \psi(\vec{v}_1)\rho(\vec{r},\vec{v}_1,t) + \nabla\cdot\int d\vec{v}_1\vec{v}_1\psi(\vec{v}_1)\rho(\vec{r},\vec{v}_1,t) = \int d\vec{v}_1\psi(\vec{v}_1)J[\rho,\rho] \ , \tag{10}$$

which can be rewritten in the form of a balance equation

$$\partial_t\overline{\psi} + \nabla\cdot\vec{j}_\psi = \partial_t^{\rm coll}\overline{\psi} \ , \tag{11}$$

describing that the time change of an averaged quantity $\overline{\psi}$ is due to flux $\vec{j}_\psi$ or due to change through collisions. The right hand side of Eq. (10) can be written as [18]

$$\int d\vec{v}_1\psi(\vec{v}_1)J[f,f] = \sigma^{d-1}\chi\int d\vec{v}_2\, d\vec{v}_1\int d\hat{\sigma} \times\Theta(\vec{v}_{12}\cdot\hat{\sigma})(\vec{v}_{12}\cdot\hat{\sigma})\rho(\vec{v}_1)\rho(\vec{v}_2)\Delta\psi \ , \tag{12}$$

and $\Delta\psi$ is the change of ψ in a direct collision for both particles $\Delta\psi = \frac{1}{2}(\psi(\vec{v}_1') + \psi(\vec{v}_2') - \psi(\vec{v}_1) - \psi(\vec{v}_2))$.

Dynamics of moments

Using Eqs. (3) and (12) the time dependence of $T(t) = \frac{m}{2}v_0^2$ in the homogeneous case is given by

$$\frac{d}{dt}T = \frac{d}{dt}\frac{m}{2}v_0^2 = -2\gamma\omega_0 T \ , \tag{13}$$

where γ is defined as

$$\gamma := -\frac{\sqrt{2\pi}}{dS_d}\frac{1}{\pi^d}\int d\vec{c}_1\, d\vec{c}_2\, d\hat{\sigma}\Theta(\vec{c}_{12}\cdot\hat{\sigma})(\vec{c}_{12}\cdot\hat{\sigma}) \times\tilde{\rho}(\vec{c}_1)\tilde{\rho}(\vec{c}_2)(b-1)\frac{1}{2}({\vec{c}_1}^{\,2} + {\vec{c}_2}^{\,2}) \ , \tag{14}$$

and $\tilde{\rho}$ as in Eq. (4). S_d is the surface of a unit sphere in d dimensions and ω_0 the Enskog collision frequency for a classical gas of hard spheres with temperature T, given by:

$$S_d = \frac{2\pi^{d/2}}{\Gamma(d/2)} \quad\text{and}\quad \omega_0 = \frac{S_d}{\sqrt{2\pi}}\chi n(2\sigma)^{d-1}v_0 \ . \tag{15}$$

If the velocity distribution function $\tilde{\rho}$ in Eq. (14) is a Maxwellian, γ takes the value of $\gamma_0 := (1-e_n^2)/(2d)$. This is the Gaussian value of the energy decay rate obtained by Haff [19]. The fact that this distribution function is not a Gaussian modifies the cooling rate, as it will be calculated later on.

In order to obtain the time evolution of a_l, we take the time derivative of Eq. (7), and it has to be considered the time dependence of $\rho(\vec{v},t)$ as well as the time dependence of $L_l^\alpha((\frac{\vec{v}}{v_0(t)})^2)$ via $v_0(t)$. The time dependence of $\rho(\vec{v},t)$ is given by Boltzmann equation, and the time dependence of $v_0(t)$ is given by equation (13). After a straight forward calculation using differential formulas for the Laguerre polynomials, we get

$$\frac{d}{dt}a_l = \omega_0\gamma_l + 2l\gamma\omega_0(a_l - a_{l-1}) \ , \tag{16}$$

and

$$\gamma_l = \frac{\sqrt{2\pi}}{S_d}\frac{1}{\binom{l+\alpha}{l}}\frac{1}{\pi^d}\int d\vec{c}_1\, d\vec{c}_2\, d\hat{\sigma}\Theta(\vec{c}_{12}\cdot\hat{\sigma})(\vec{c}_{12}\cdot\hat{\sigma}) \times\tilde{\rho}(\vec{c}_1)\tilde{\rho}(\vec{c}_2)(b-1)\frac{1}{2}(L_l^\alpha(\vec{c}_1^{\,2}) + L_l^\alpha(\vec{c}_2^{\,2})) \ . \tag{17}$$

All collision integrals γ and γ_l depend on a_l for all l via $\tilde{\rho}$. We mention here that our approach is equivalent to the dynamics proposed in [11], but has the advantage to give immediately the explicit time dependence of all coefficients, at least formally.

Collision frequency

The set of equations (13) and (16) for T and a_l with γ_l and γ given by (17) and (14) are the main results of this paper. However, before analyzing them in detail in the next section and comparing them with computer simulations in Sec. 5, it is instructive to study the collision frequency ω. In order to do so, we introduce the average number of collisions, τ, that a particle has suffered in a time t. Then, the collision frequency is defined as $\omega = \frac{d}{dt}\tau(t)$. In elastic fluids ω is a constant number depending only on the density and temperature, so that τ and t are proportional quantities. In granular fluids, however, ω depends on time, as the temperature (and more precisely also the shape of the distribution function) of the system changes with time. Therefore, it is more natural from a physical point of view to express the time evolution equations in terms of the variable τ rather than t. Moreover, the hydrodynamic matrix become time independent when the hydrodynamic equations are expressed in the variable τ [8].

To determine $\omega = \frac{d}{dt}\tau(t)$ we use Eq. (12) and the fact that in each collision the number of collisions that each particle has suffered increases by one and we obtain [18]

$$\frac{d}{dt}\tau = \omega_0\gamma_\tau \ , \quad\text{and} \tag{18}$$

$$\gamma_\tau = \frac{\sqrt{2\pi}}{S_d}\frac{1}{\pi^d}\int d\vec{c}_1 d\vec{c}_2\, d\hat{\sigma}\Theta(\vec{c}_{12}\cdot\hat{\sigma})(\vec{c}_{12}\cdot\hat{\sigma})\tilde{\rho}(\vec{c}_1)\tilde{\rho}(\vec{c}_2) \ . \tag{19}$$

γ_τ depends on all a_l and for the case that all $a_l = 0$ for $l > 1$ we would get $\gamma_\tau = 1$ and thus the Enskog value ω_0. We define a time $\tilde{\tau}$ by

$$d\tilde{\tau} = \omega_0 dt \ . \tag{20}$$

Note that $\tilde{\tau}$ is only an approximation of τ defined in Eq. (18), so it does not really measure time in collisions, but we will show later that the deviations of $\tilde{\tau}$ from τ remain small for not too high inelasticities. In other words we hope that the collision frequency is approximately determined by the Enskog value and corrections due to deviations from the Gaussian affecting the collision frequency are small.

Cooling rate

How can the dynamics be described in a state where all coefficients have already reached their asymptotic values?

Note that the quantities γ and γ_τ are entirely given by the values of a_l. Assuming that all a_l have reached their asymptotic values for some time $t > t^*$ or equivalently $\tau > \tau^*$ the quantities γ and γ_τ also remain constant and we denote their asymptotic values by γ^* and γ_τ^*. Then we consider Eq. (13) and (18):

$$\frac{d}{dt}T = -2\gamma^*\omega_0(T)T \ , \tag{21}$$

$$\frac{d}{dt}\tau = \omega_0(T)\gamma_\tau^* \ , \tag{22}$$

which is solved analytically

$$\begin{aligned} T &= \frac{T(t^*)}{\left[1+\gamma^*\omega_0\big(T(t^*)\big)\big(t-t^*\big)\right]^2} \\ &= T(\tau^*)\exp\left(-2\gamma^*/\gamma_\tau^*(\tau-\tau^*)\right) \ , \end{aligned} \tag{23}$$

so that

$$\tau(t) - \tau^* = \frac{\gamma_\tau^*}{\gamma^*}\ln\left[1+\gamma^*\omega_0\big(T(t^*)\big)\big(t-t^*\big)\right] \ . \tag{24}$$

Eq. (24) provides a relation between collisional time and real time. Eq. (23), i.e. the algebraic decay of the temperature in time or the exponential behavior in τ is called Haff's law. Furthermore, this equation makes explicit the fact that the shape of the velocity distribution function modifies the energy decay rate.

4 Analytical results

Truncation scheme

Up to now we have determined the *full* time dependence of the HCS in terms of the time dependence of all its moments in Eqs. (13) and (16). This infinitely large system of differential equations can only be solved by truncation. The approximate solution found by truncation only makes sense if all neglected terms are *small* as compared with the remaining ones. On the other hand, for small inelasticities the velocity distribution function is close to a Gaussian, so that $a_2 \ll 1 = a_0$. We generalize this unequality and assume that $a_{l+1} \ll a_l$ for all l, i.e. contributions from higher order coefficients get smaller the higher the index. Therefore, we propose a truncation scheme in which we assume that a_l is of order λ^l, where λ is a small parameter. If we now make "an approximation of order $\mathcal{O}(\lambda^l)$" we neglect *all* terms in *all* considered equations higher than λ^l. This truncation scheme produces a finite set of differential equations that can be solved.

We will concentrate on two aspects: (i) To investigate the *dynamics* we integrate the full set of *differential* equations (up to a certain order λ). The *asymptotic* values of the coefficients can then be obtained by taking the long-time limit if they become stationary in time. (ii) To discuss the stationary state we set the left hand side of Eq. (16) equal to zero. This set of coupled and, as the case may be, non-linear equations can be solved with the numerical tool provided by the computer algebra program. Note that not all of these *stationary* values are necessarily dynamically stable solutions of the corresponding differential equation.

Results to order 2

In a first step we only take into account a_2 to linear order. Then the functional form of the equation for a_2 Eq. (16) is given by

$$\frac{d}{dt}a_2 = \omega_0(\gamma_2 + 4\gamma a_2) \to \frac{d}{d\tilde{\tau}}a_2 = \gamma_2 + 4\gamma a_2 \ . \tag{25}$$

Again, the use of $\tilde{\tau}$ simplifies the form of the equations, as it eliminates the time dependent factor ω_0. We recall here that both γ_2 and γ depend on all a_l, but for the approximation treated here, they only depend on a_2 in a linear manner. Therefore, we can express Eq. (25) as

$$\frac{d}{d\tilde{\tau}}a_2 = A + Ba_2 + \mathcal{O}(\lambda^3) \ , \tag{26}$$

where A and B are constants given by the collision integrals in γ and γ_2 with the explicit expressions in two dimensions: $A = \frac{1}{8}(e_n^2-1)(2e_n^2-1)$ and $B = \frac{1}{128}(30e_n^4 - 5e_n^2 - 32e_n - 57)$.
(i) Dynamics – The evolution equation (26) for a_2 where time is expressed in collisions per particle is linear in a_2, so it can be easily integrated to give, when $a_2(0) = 0$,

$$a_2(\tilde{\tau}) = -\frac{A}{B}(1-\exp(B\tilde{\tau})) \ , \tag{27}$$

so that the asymptotic value of a_2 is reached exponentially fast on a time scale of the order of $\tilde{\tau}_0 := -B^{-1}$. The decay time $\tilde{\tau}_0$ ranges between 1.7 and 2.25. As an important consequence the asymptotic solution is quickly reached on a kinetic time scale of few collisions per particle.
(ii) Stationary state – For times larger than $\tilde{\tau}_0$ a_2 reaches the stationary value of $-A/B$ which coincides with the values calculated in [10].

Results to order 3

To keep the discussion simple and to compare results from order to order, we first take into account only a_2 and a_3 i.e. up to $\mathcal{O}(\lambda^3)$. We then still have to deal with equations which are linear in the coefficients (a_2^2 is already of order $\mathcal{O}(\lambda^4)$). In the next section we will discuss the non-linear case up to order $\mathcal{O}(\lambda^6)$. The equations read

$$\begin{aligned} &\frac{d}{dt}T = -2\gamma\omega_0 T, \\ &\frac{d}{dt}a_2 = w_0\gamma_2 + 4\gamma\omega_0(a_2 - 0), \\ &\frac{d}{dt}a_3 = w_0\gamma_3 + 6\gamma\omega_0(a_3 - a_2), \\ &\frac{d}{dt}\tau = \omega_0\gamma_\tau, \\ &\frac{d}{dt}\tilde{\tau} = \omega_0 \quad \text{neglecting corrections of } a_2 \text{ and } a_3 \ . \end{aligned} \tag{28}$$

We use computer algebraic programs to calculate the collisions integrals γ, γ_l and γ_τ up to order $\mathcal{O}(\lambda^3)$. The analytical solutions are rather lengthy and we will only show here results for a system with $e_n = 0.9$ in Figs. 1–3.
(i) Dynamics – We have solved the simultaneous Eqs. (28) numerically[1] for the case $e_n = 0.9$ and in the following we

[1] We have used the built-in numerical procedure `dsolve` of MAPLE to integrate the differential equation.

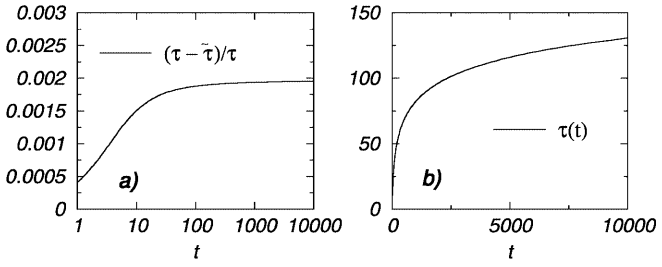

Fig. 1a, b. a Relative deviations of collisions per particle from the approximation given by the Enskog value as a function of time. **b** Collisions per particle as a function of time. Dissipation, $e_n = 0.9$

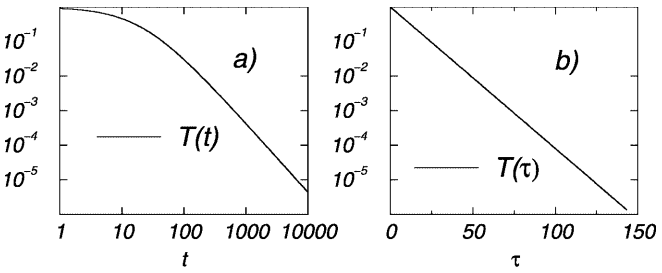

Fig. 2a, b. Temperature as a function of time **a** and collisions per particle **b**. Dissipation, $e_n = 0.9$

always plot time in units of $1/\omega_0(T(0))$ and temperature in units of $T(0)$. We have chosen $a_2(0) = a_3(0) = 0$ as initial condition. In a first step we proof that the approximation to use $\tilde{\tau}$ instead of τ can be justified (at least to this order). In Fig. 1 a) we show the relative deviations of the true number of collisions to the approximation given by the Enskog Boltzmann value, i.e $(\tau - \tilde{\tau})/\tau$ as function of time in a semilogarithmic plot.

We see that the relative deviations remain smaller than 0.2%. This allows us, at least in the homogeneous cooling state, to use $\tilde{\tau}$ instead of τ in Eqs. (23) and (24).

In the asymptotic state we get $\gamma^* = 0.04723$ for $e_n = 0.9$ and values from the numerical integration of Eqs. (28) coincide with Eqs. (23) and (24) within the graphical accuracy, so we plotted here only the numerical solution. Fig. 1 b) shows $\tau(t)$ which has the same form as predicted in Eq. (24).

In Fig. 2 a), we show T as a function of time in a double logarithmic plot. We see the well-known asymptotic time dependence $T \propto t^{-2}$. In Fig. 2 b), we show T as a function of τ in a semi logarithmic plot resulting in a straight line with slope $-2\gamma^*$ as predicted by Eq. (23).

In Fig. 3 we show the time dependence of a_2 and a_3 as a function of time a) and as a function of τ b).

We see that a_2 and a_3 reach their asymptotic value on a very short time scale which is of the order of few τ's. Therefore, few collisions per particle are necessary to reach the asymptotic state for a_2 and a_3.

(ii) Stationary state – As mentioned above we calculate the stationary values by setting the l.h.s of Eq. (28) equal to zero. In Fig. 4 we show the results for the stationary values of a_2 and a_3 to $\mathcal{O}(\lambda^3)$ as well as a_2 to $\mathcal{O}(\lambda^2)$.

As long as $e_n > 0.6$, a_2 to $\mathcal{O}(\lambda^2)$ does not differ significantly from a_2 to $\mathcal{O}(\lambda^3)$ and a_3 remains small. We see stronger differences for smaller e_n and a_3 becomes as important as a_2 which indicates stronger deviations from the Gaussian state. We also cannot assume anymore that corrections of higher orders remain small since we do not have any indication that the series is converging in the sense that the $|a_l|$ are small and decreasing.

Since to $\mathcal{O}(\lambda^3)$ we have to deal with a set of linear equations we only find one unique solution. Considering higher orders one will find many solutions whose validity must be investigated. We will discuss this problem in the next section.

Results to order 6

In this section we go to $\mathcal{O}(\lambda^6)$, which is the highest order we were able to calculate with the computer algebra program.

(i) Dynamics – In Fig. 5 we show for $e_n = 0.8$ the dynamics for the 5 non-vanishing coefficients $a_2, \ldots, a_6$ as a function of time. We have chosen the initial condition $a_2(0) = \cdots = a_6(0) = 0$. We see again a very fast decay to their asymptotic values. We observe that $|a_l| > |a_{l+1}|$ and in this sense the perturbation expansion seems to converge.

(ii) Stationary state – We calculate the stationary values

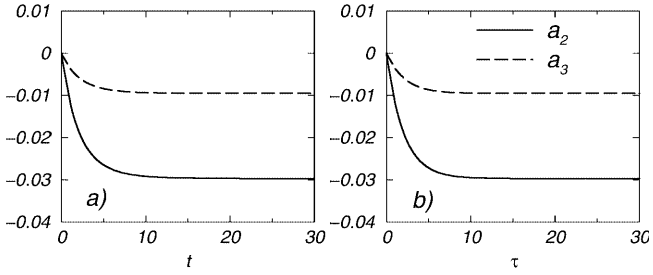

Fig. 3a, b. Coefficients a_2 and a_3 as a function of time **a** and collisions per particle **b**. Dissipation, $e_n = 0.9$

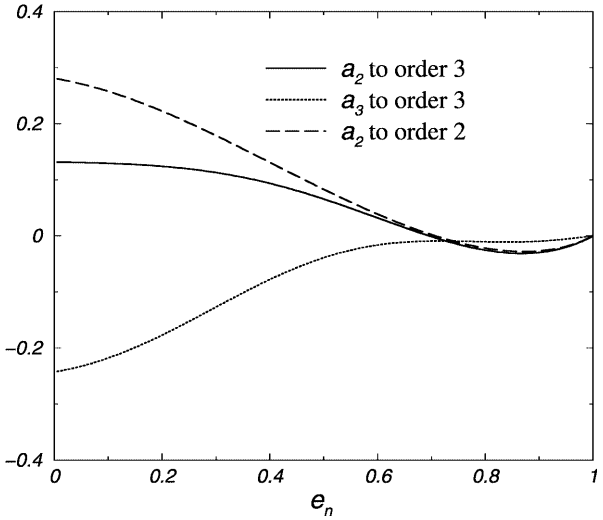

Fig. 4. Coefficients a_2 to $\mathcal{O}(\lambda^2)$, and a_2 and a_3 to $\mathcal{O}(\lambda^3)$ as a function of e_n

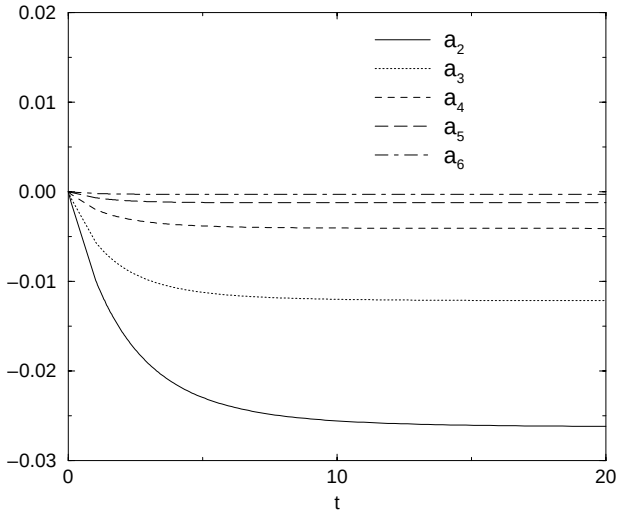

Fig. 5. The coefficients $a_2, \ldots, a_6$ calculated to order $\mathcal{O}(\lambda^6)$ as a function of time for $e_n = 0.8$

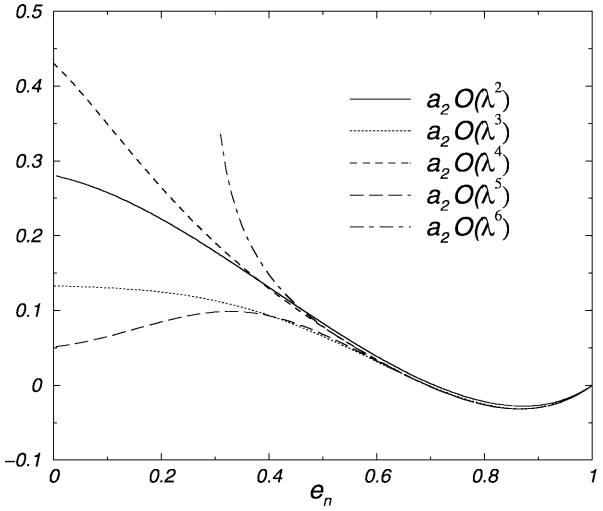

Fig. 7. Stationary value of a_2 to order $\mathcal{O}(\lambda^3)$ up to $\mathcal{O}(\lambda^6)$ as function of e_n

by setting the l.h.s of Eq. (16) equal to zero. In Fig. 6 we show the results of the stationary values as a function of $e_n > 0.3$.

For $e_n > 0.7$ the coefficients remain small and the expansion seems to converge in the sense that $|a_l| > |a_{l+1}|$ for all l. For $e_n < 0.7$ the absolute values of the coefficients start to grow and seem to diverge with e_n approaching 0.3.

To discuss the validity of these results we compare in Fig. 7 the asymptotic values of a_2 of order $\mathcal{O}(\lambda^2)$ up to order $\mathcal{O}(\lambda^6)$. As long as $e_n > 0.6$, we do not find significant differences between the two orders, only the first order differ slightly from the other ones. This is a further hint that for these values of e_n the perturbation method works. Moreover, the ratios of a_{l+1}/a_l are small and of the same order: for instance, for $e_n = 0.85$, these ratios are: $a_3/a_2 = 0.39$, $a_4/a_3 = 0.29$, $a_5/a_4 = 0.24$ and $a_6/a_5 = 0.16$.

For $e_n < 0.6$ the results differ drastically from order to order and the proposed truncation scheme for Eq. (16) fails. We conjecture that around $e_n \approx 0.6$ an essential change in the distribution function occurs. Then the distribution function is no more described by small deviations around a Gaussian and might be better expressed by an expansion around an exponential as suggested in [4] and confirmed by DSMC simulations of [14]. We will go back to this point at the end of Sec. 5.

In view of Fig. 7, another possible explanation for the failure of the convergence is that the expansion in λ is of asymptotic type, in such a way that including higher orders the expansion would break down in the whole range $0 < e_n < 1$. Unfortunately, we cannot decide which is the correct option, as we can only calculate up to order $\mathcal{O}(\lambda^6)$.

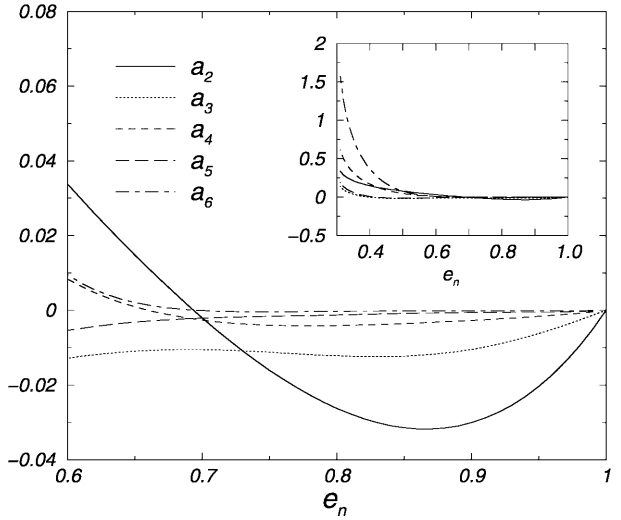

Fig. 6. Stationary values $a_2, \ldots, a_6$ calculated to order $\mathcal{O}(\lambda^6)$ as a function of e_n

Further unstable solutions

Since we have to deal with non-linear equations, the solution is not unique and e.g. for $e_n = 0.8$ two further stationary solutions can be found, similar as in [11]. We list the values of the other coefficients for these stationary solutions:

	Solution 1	Solution 2
a_2	8.95	−24.62
a_3	−14.39	−4.50
a_4	59.11	39.53
a_5	−109.17	178.6
a_6	127.8	−197.7

Both solutions are dynamically unstable which we have shown by numerical integration of the corresponding differential equations (13) and (16). In addition we observe that the higher coefficients are not at all negligible so that our assumptions, which should allow us to truncate the system of differential equations, are severely violated. Hence for these cases we can assume that we have not even found an approximate solution of the homogeneous Boltzmann equation.

5 Computer simulation results

In the literature only Direct Simulation Monte Carlo methods (DSMC) have been used for measuring the values of a_2 and a_3 [12] and a_2 agrees very well with the value calculated in [10]. However, DSMC lacks some features of the real IHS fluid, as correlations among the particles.

We present in this paper for the first time results for a_2 and for high-energy tails obtained from Molecular Dynamics (MD) simulations of the IHS system in 2 dimensions. Our code closely follows the event driven molecular dynamics code presented in [20], adapted to the collision rules described in Eqs. (1) and accelerated by techniques described in [21]. Typical simulations are performed with $N = 50000$ particles in a square box of size L, being its area fraction $\phi = \frac{\pi\sigma^2}{4}n = \frac{\pi N\sigma^2}{4L^2}$. The initial configuration is that of an elastic fluid at equilibrium (Maxwellian distribution for velocities and equilibrium correlations for the positions due to excluded volume effects), prepared by running the system with $e_n = 1$ (elastic interactions) for not less than 50 collisions per particle. Therefore, in the initial state $a_l = 0$ for $l \geq 1$.

At the beginning of the inelastic evolution the system remains for some time in the HCS, where the assumptions made in Sec. 2 are fully applicable and where computer simulations will serve to test those predictions. Later, vortices and clusters start to develop through the system and homogeneity is lost [1,6]. The higher the density ϕ and the inelasticity the sooner these structures appear and important deviations from the theoretical values of a_l are expected. We will come back to this point later. Furthermore, the analytical results are *independent* of the density[2] when expressed in τ, but only depend on the inelasticity e_n. Hence we have performed our simulations at low density of $\phi = 0.05$, although simulations at higher and lower densities have also been carried out.

Results for moments

The typical time evolution of the 4th cumulant is shown in Fig. 8, where we have plotted the value of a_2 versus the number of collisions per particle τ for a low density case $\phi = 0.05$ and low inelasticity $e_n = 0.92$. The dotted line is the result of Eq. (27) while the solid line is the result of the numerical simulation averaged over two realizations to slightly improve the accuracy. In this plot we observe the typical features of the IHS evolution described in former sections. Initially a_2 is equal to zero, as the system starts from a Maxwellian distribution, with $a_l = 0$ for $l > 1$. Then, within a very short time of a few collisions per particle, deviations from a Maxwellian build up in the system and the asymptotic values of a_l are reached. This is a very fast process on a hydrodynamic time scale, as it involves only a few collisions per particle and, therefore, a few mean free times. Then the moments stay constant (within the accuracy of the computer simulations) as long as the system remains in the HCS.

[2] To eliminate the dependency of real time on the density, time can be scaled by the collision frequency $\omega(T(0))$ at time $t = 0$.

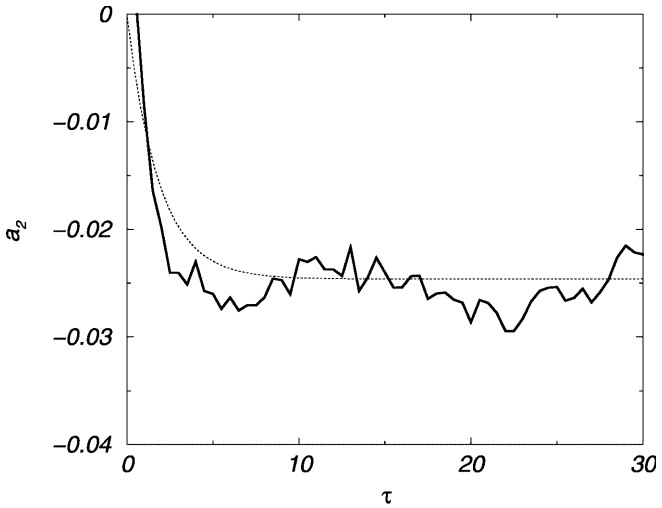

Fig. 8. Time evolution of a_2 for an IHS system with $\phi = 0.05$ and $e_n = 0.92$. The dotted line is the analytical result, while the solid line is the numerical simulation data averaged over two realizations

A best fit of the simulation data to an expression like Eq. (27) gives that $\tilde{\tau}_0 = 1.6 \pm 0.5$ and $a_2(\infty) = -0.026 \pm 0.004$, while the theoretical values developed in Sec. 4 are $\tilde{\tau}_0 = 1.85$ and $a_2(\infty) = -0.0246$. We observe excellent agreement with the theory. Unfortunately, the accuracy of our computer simulations is not high enough to distinguish between the lowest order and the order 6. The DSMC method also finds good agreement with the value of a_2 [12].

At later times the system is no longer in the HCS and the assumptions used in the theoretical sections break down. This is best illustrated in the Fig. 9, where a simulation at low density $\phi = 0.03$ but at very high inelasticity $e_n = 0.4$ is presented. We observe the same features described in Fig. 8 with values from simulations $\tilde{\tau}_0 = 1.5 \pm 0.5$ and $a_2(\infty) = 0.125 \pm 0.007$, a best fit

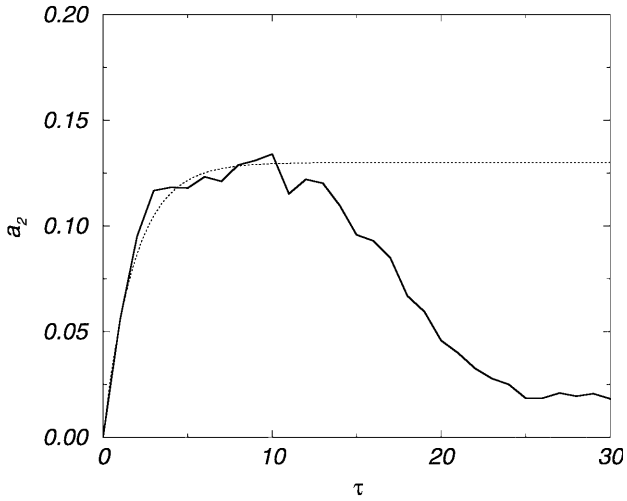

Fig. 9. Time evolution of a_2 for an IHS system with $\phi = 0.03$ and $e_n = 0.4$. The dotted line is the analytical result, while the solid line is the numerical simulation data averaged over two realizations. Deviations from HCS are seen after $\tau > 12$

for $\tau < 10$, compared to the theoretical values $\tilde{\tau}_0 = 1.83$ and $a_2(\infty) = 0.130$. Again, the agreement is excellent. However, after a short time $\tau \gtrsim 12$ the values of the moments start to deviate from the theoretical predictions. For $\tau \gtrsim 12$ the homogeneity assumption breaks down. This can be checked, e.g. by plotting the curve of energy vs time [2,5]: deviations from Haff's law imply lack of homogeneity [7,22]. Visual inspection of the system (not presented here) show that, at this high inelasticity, the system immediately develops currents and dense clusters where particles move almost parallel inside them. The description in terms of $\tilde{\rho}(c)$ is wrong, as it does not take into account the local macroscopic currents. The values of a_2 can, at this late evolution stages, grow up to values of $a_2 = 2$ [2]. This regime is outside the scope of this article.

Concerning the duration of HCS, a hydrodynamic analysis [7] shows that currents develop through the system on a time scale of τ of the order of γ_0^{-1}. In Fig. 8 the deviation with respect to $a_2(\infty)$ appears at $\tau \simeq 35 = 1.3\gamma_0^{-1}$, while in Fig. 9 it appears at $\tau \simeq 12 = 2.5\gamma_0^{-1}$.

The results of the MD simulations for a_2 in the HCS compared with the asymptotic solution of Eq. (26) are given in Fig. 10. The agreement is excellent even down to high inelasticities as $e_n = 0.4$, as shown in Fig. 9. However our simulations do not have precision enough to test if higher order corrections are important. Concerning the values of $\tilde{\tau}_0$, MD results are very close, but always smaller than the theoretical values quoted below Eq. (27) and they are affected by large errors.

To conclude this section, we have also measured the 6th moment, $\langle c^6\rangle = \langle v^6\rangle/\langle v^2\rangle^3$, and from this quantity we have obtained a_3 given by $a_3 = -\frac{1}{6}\langle c^6\rangle + (1+\frac{d}{4})\langle c^4\rangle + (\frac{d^3}{48} - \frac{7d}{12} - 1)$. The results also agree with the solutions of Eq. (28), but, as expected, the discrepancies are now larger because the absolute value of a_3 is very small.

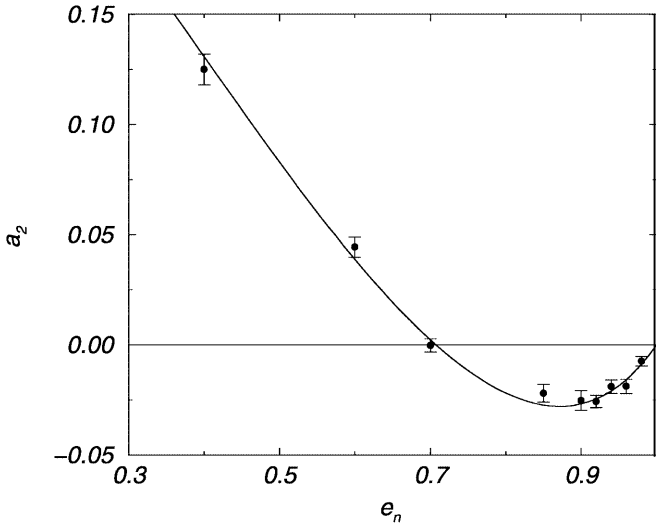

Fig. 10. Coefficient a_2 versus the coefficient of restitution e_n. The solid line is the theoretical prediction of Eq. (26) and the circles are the values calculated from MD simulations with their corresponding error bars

Cooling rate

Another way to test the analytical results of Sec. 4 is to measure the dissipation rate given by the decay of the temperature T or energy E versus τ. Haff's calculations predicts an exponential law $\exp(-2\gamma_0\tau)$ with $\gamma_0 = (1-e_n^2)/2d$ while higher order corrections modify it as shown in Eq. (23). These corrections respect to γ_0 are very small of only few parts in a thousand. If the IHS system is too large or inelastic, these deviations cannot be measured, as the curve of energy vs τ bends apart of the exponential law [5,22]. This is due to the appearance of currents and vortices as quantitatively explained by [22]. Moreover, temperature and energy are no longer proportional, and, in contrast to energy, temperature is difficult to measure in a numerical experiment.

However, if the system is small enough no shear or clustering instability is excited (see e.g. Refs. [5,7] for detailed explanations) and the system is forced to remain in the HCS for all times, where Eq. (23) is valid. This is called 'kinetic regime' in Ref. [5]. The drawback of this method is that, for a given density, it sets a *maximum* number of particles, that decreases with increasing inelasticity. As described in Ref. [7] a lower bound for $k_{min} = \frac{2\pi}{L} < k_\perp^*$ has to be satisfied, in the notation of [7]. We keep $k_{min} = 2k_\perp^*$. This condition, together with our chosen low density of $\phi = 0.05$, restricts the number of particles to $N = 80$ at $e_n = 0.70$, and the results are no longer reliable. Even for $e_n = 0.95$ the maximum number of particles is only $N \simeq 300$. Hence we restrict ourselves to $e_n > 0.7$.

Following this method we have performed simulations and have measured the energy decay rate as a function of τ. We have verified that it is indeed exponential for all times, and, in order to improve the statistics, results are averaged over 1000 realizations. The results are presented in Fig. 11, where we plot the difference between the stationary energy decay rate γ^*/γ_τ^* from Eq. (23) and γ_0. Circles are data obtained by MD simulations with their errors bars, while dotted and dashed lines are the results from our theory to order $\mathcal{O}(\lambda^2)$ and $\mathcal{O}(\lambda^3)$ respectively. The small number of particles does not allow to obtain

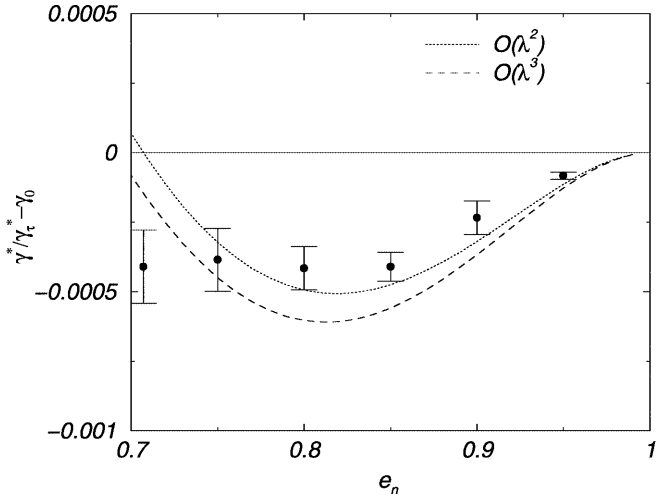

Fig. 11. Deviations of the cooling rate as a function of the inelasticity as obtained in simulations of small systems that remain in the HCS

any significant result below $e_n < 0.7$. For $e_n > 0.75$ we observe a reasonable agreement, although we find significant deviations with respect to the theoretical results, MD data are always smaller that theoretical values. Unfortunately, no direct measurements with DSMC of the deviations respect to γ_0 have been reported so far. They would allow us to compare our results and elucidate the nature of these deviations.

It is important to note here that due to the small size of the deviations of the cooling rate with respect to γ_0 it is necessary to use in the theory the real number of collisions τ instead of $\tilde{\tau}$. The approximation $\tilde{\tau} \simeq \tau$ is correct within a few parts in a thousand as shown in Sec. 4, which is of the same order of magnitude as the correction γ^*/γ_τ^* with respect to γ_0. This is not the case, however, for calculations of the dynamics of a_l, for example given in Eq. (27), where we are not interested in such small deviations but want to give a first estimate of the time scales. Hence the use of $\tilde{\tau}$ and the approximation made in Eq. (27) is fully justified.

Finally, there is still the open question if deviations from the theoretical a_2 and the cooling rate are due to the existence of correlation in the HCS and the breakdown of the *molecular chaos* hypothesis in Eq. (8) reported in [23, 24]. These effects cannot be tested in DSMC either, as this method is based on the factorization of the two particle distribution function.

High-energy tails

In Refs. [4,10] it has been shown that strong deviations with respect to the Maxwellian are present in the tails of the distribution, where particles have large energies. More precisely, they have found if $c = v/v_0(t) \gg (1-e_n^2)^{-1}$ the velocity distribution function is no longer Maxwellian, but a simple exponential $\tilde{\rho} \simeq \mathcal{A}\exp(-Ac)$ instead. This exponential distribution has been verified by numerical solutions of the Boltzmann equation using the DSMC method [14]. The shape of the exponential is very different to the Maxwellian and therefore it is understandable that an expansion of the type given in Eq. (4) might be non-convergent as suggested by our theoretical analysis. Another reasonable possibility is that the series is indeed convergent but we have not gone high enough in the truncation scheme or there is a better choice of truncation, because a_{l+1} is as large as a_l, as shown in Fig. 6.

In order to investigate the velocity distribution function and make the exponential range accessible, we have performed MD simulations with extreme inelasticities of $e_n = 0.1, 0.2, 0.4$ to compare to moderate inelasticities 0.6 and 0.8. Moreover, as we need high accuracy in the tails, where populations are small, we have simulated systems with 250 000 particles at $\phi = 0.05$. However, even with this large number of particles we are not able to obtain the accuracy that can be achieved by the DSMC method [14]. We will only be able to give evidences of the exponential tail. We measured the distribution function at times, where a_2 has already reached its asymptotic value, but the homogeneity assumption is still valid. In the example of Fig. 9 this would be at times $5 \lesssim \tau \lesssim 10$.

To estimate the distribution function from data, we use the kernel estimator technique described e. g. in [25]. In general, given a set of outcomes $x_i,\ i = 1, \ldots, M$ of a random experiment the distribution function $\rho(x)$ can be estimated by

$$\rho(x) \simeq \frac{1}{M}\sum_{i=1}^{M} \frac{1}{\sqrt{2\pi}\delta} \exp\left(\frac{(x_i - x)^2}{2\delta^2}\right) \quad . \tag{29}$$

The idea behind this method is that each data point also gives some information about its surrounding, which can be justified for smooth distribution functions. It is not necessary to use a Gaussian as kernel in Eq. (29), any normalized and more or less sharply peaked function can be used. The value δ is a free parameter which was chosen such that the measured distribution function for the elastic gas (i.e. the initial condition) is fitted best (to the eye) to the Maxwellian. We choose $\delta = 0.05$. Since the distribution function $\tilde{\rho}(c^2)$ – with c the modulo of the velocity – is not continuous at $c = 0$, i.e. $\tilde{\rho} = 0$ for $c < 0$ and $\tilde{\rho}(0) \approx 1/\pi$ this technique gives bad results around $c = 0$, but better results than the histogram method for the interesting high-velocity limit, where only few data points are given.

The simulation results for the velocity distribution function $\tilde{\rho}$ as a function of c as well as the Maxwellian are shown in Fig. 12 in a semi-logarithmic plot. For $c \gtrsim 3.5$ the statistical accuracy is poor, so results are only plotted up to $c = 3.5$.

We observe that the deviations with respect to the Maxwellian are larger for lower values of e_n. On the contrary, as e_n increases, the measured distribution approaches the Maxwellian. Closer inspection shows that for $e_n = 0.1$ the distribution gets possibly close to an exponential (straight line in the semilogarithmic plot of Fig. 12) for $2 \lesssim c \lesssim 3.5$, while for $e_n = 0.6$ the range where $\log\tilde{\rho}$ seems to be linear shrinks to $3 \lesssim c \lesssim 3.5$. We will show below that in this case ($e_n = 0.6$ and $c \lesssim 3.5$) the distribution function can be reasonably well described by the results of the perturbation expansion around the Gaussian given in Eq. (4). If we perform a linear fit to an exponential in these ranges, we obtain values of the coefficient A quite

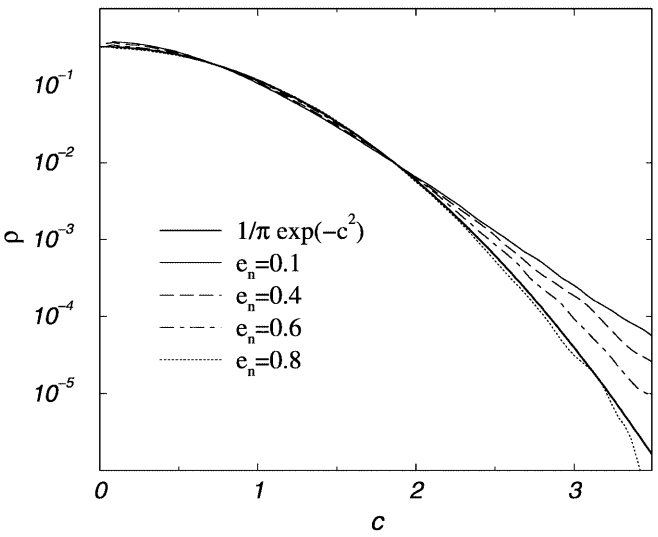

Fig. 12. Maxwellian and measured velocity distribution function $\tilde{\rho}$ as a function of c for various values of e_n

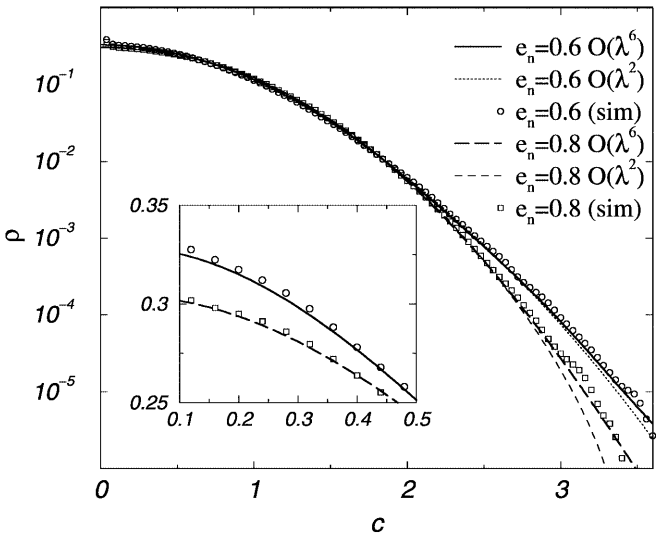

Fig. 13. Measured velocity distribution function $\tilde{\rho}$ as a function of c for $e_n = 0.6$ and $e_n = 0.8$ compared to results of Sec. 4 to orders λ^2 and λ^6. The inset shows an blow up of the results for small velocities

close to those reported by [10], tested in [14] by DSMC method. For instance, for $e_n = 0.1$, $A \simeq -3.2$, that increases to $A \simeq -3.8$ at $e_n = 0.4$ and further to $A \simeq -4.7$ at $e_n = 0.6$.

If we go beyond $e_n > 0.6$ the perturbation expansions of Sec. 4 seems to converge and it make sense to compare the analytical results with the simulation data. In Fig. 13 we show for $e_n = 0.6$ and $e_n = 0.8$ results of the simulations and of the analytical theory to orders λ^2 and λ^6.

In the whole range of c which is plotted, the analytical results to order λ^6 coincides fairly well with the measured data. However, results to order λ^2 agree at small velocity, $c \lesssim 3$ for $e_n = 0.8$, but fails for higher velocities. It seems reasonable that higher orders are needed to describe higher energy tails, where deviations respect the Gaussian are larger.

Therefore, for $e_n > 0.6$ there is no need to describe data by an exponential tail for high velocities, although it cannot be assured, that the theory does not fail for even higher velocities. Note that the distribution function at $c \approx 3.5$ is already smaller than 10^{-5} so that for 250 000 particles only 2 or 3 particles might not be correctly described.

6 Conclusion

In this article we investigated by means of analytical theory and simulations the dynamics of a freely cooling system of smooth granular particles as long as it remains homogeneous. Starting from a pure Gaussian state the system develops on a fast time scale to a state where the deviations from the Gaussian (described by cumulants) are stationary in time and the dynamics is entirely described by a decreasing kinetic energy.

More technically, we determined formally the *full* dynamics of the homogeneous cooling state in terms of the dynamics of the temperature $T(t)$ and the *time dependent* coefficients $a_l(t)$ of an expansion of the velocity distribution function in Generalized or Associated Laguerre polynomials around the Gaussian state. We obtained an infinitely large system of non linear ordinary differential equations, which can be solved numerically under the assumption that higher coefficients do not contribute.

Analytically, we found two main results. i) As far as dynamics is concerned, the HCS is characterized by the fact that only a few collisions per particle are necessary to reach a state where the coefficients are stationary in time. Then the entire time dependence is given by a slow algebraically decay of the temperature obeying $\frac{d}{dt}T = -2\omega_0\gamma T$, with γ depending on all the asymptotic values of the coefficients a_l. ii) As far as the asymptotic values of the coefficients are concerned, the expansion seem to converge in the sense that $|a_{l+1}| < |a_l|$ for $e_n > 0.6$ and for this range of e_n we do not find significant differences between orders. There exist further stationary but dynamically instable solutions of the considered differential equation, which are far away from the assumption of absolutely decreasing and small coefficients, so we cannot make any prediction for that cases. For $e_n < 0.6$ the perturbation procedure seems to fail, the assumption we made to truncate the system of differential equations are severely violated and we find a strong dependency on the order of approximation. We have no answer if going to higher order or choosing a more suitable truncation scheme would show that the perturbation procedure nevertheless works, or, on the other hand, if the expansion presented here is only of an asymptotic type. A reasonable conclusion is that the system develops to a state which is very far from a Gaussian and might be better described by an expansion around an exponential as discussed in [11] and [12].

Although much numerical work has been done on the HCS and clustering regimes (see, e.g. [1], [5], [7], [23] and [26]), for the first time event-driven simulations are used in the present work to investigate deviations from the Gaussian distribution in the HCS. Mainly, three aspects were considered: 1) The dynamics and asymptotic values of the coefficients, 2) the influence on the decay rate of the temperature, 3) the shape of the velocity distribution function.

1. As long as the system remains in the homogeneous state the dynamical behavior as well as the static value of a_2 could be confirmed. Nevertheless, the statistics was too poor to distinguish if higher order analytical results give better values.
2. Similarly, the decay of the temperature was measured showing deviations with respect to the analytical results and opening the possibility to study other effects as correlations. Here we had to assure that the system remains in the homogeneous state, restricting the number of particles and therefore the quality of the statistics.
3. Measuring the full velocity distribution function we found that the distribution function can be described very well by the expansion around the Gaussian as long as $e_n > 0.6$. For smaller e_n the high-energy tails show an exponential shape confirming previous results found by analytical theory [4,10] and DSMC simulations [14].

A possible extension of our work are systems of rough spheres with constant coefficient of restitution or Coulomb friction. Strong deviations from the Gaussian are observed in the angular velocity distribution function, surprisingly for the cases where the particles are almost *smooth* [27, 28]. It would be interesting to perform a similar dynamical analysis along these lines.

References

1. I. Goldhirsch & G. Zanetti, Clustering instability in dissipative gases. Phys. Rev. Lett. 70 (1993), p. 1619
2. I. Goldhirsch, M.-L. Tan & G. Zanetti, Molecular dynamical study of granular fluids I: the unforced granular gas in two dimensions. J. Sci. Comput. 8 (1993), p. 1
3. P. Deltour & J. L. Barrat, Quantitative study of a freely cooling granular medium. J. Phys. I France 7 (1997), p. 137
4. S. E. Esipov & T. Pöschel, The granular phase diagram. J. Stat. Phys. 86 (1997), p. 1385
5. S. McNamara & W. R. Young, Dynamics of a freely evolving, two-dimensional granular medium. Phys. Rev. E 53 (1996), p. 5089
6. T. P. C. van Noije, M. H. Ernst, R. Brito & J. A. G. Orza, Mesoscopic theory of granular fluids. Phys. Rev. Lett. 79 (1997), p. 411
7. J. A. G. Orza, R. Brito, T. P. C. van Noije & M. H. Ernst, Patterns and long range correlations in idealized granular flows. Int. J. Mod. Phys. C 8 (1997), p. 953
8. T. P. C. van Noije, M. H. Ernst & R. Brito, Spatial correlations in compressible granular flows. Phys. Rev. E 57 (1998), R4891. T. P. C. van Noije & M. H. Ernst, Cahn-Hilliard theory for unstable granular fluids. Phys. Rev. E 61 (2000), p. 1765
9. A. Goldshtein & M. Shapiro, Mechanics of collisional motion of granular materials. Part 1. General hydrodynamic equations. J. Fluid Mech. 282 (1995), p. 75
10. T. P. C. van Noije & M. H. Ernst, Velocity distributions in homogeneously cooling and heated granular fluids. Gran. Matt. 1 (1998), p. 57
11. N. V. Brilliantov & T. Pöschel, Deviation from Maxwell distribution in granular gases with constant restitution coefficient. Phys. Rev. E 61 (2000), p. 2809
12. J. J. Brey, M. J. Ruiz-Montero & D. Cubero, Homogeneous cooling state of a low-density granular flow. Phys. Rev. E 54 (1996), p. 3664
13. N. V. Brilliantov & T. Pöschel, Velocity distribution in granular gases of viscoelastic particles. cond-mat Phys Rev E, 61, 2000, p. 5573
14. J. J. Brey, D. Cubero & M. J. Ruiz-Montero, High energy tail in the velocity distribution of a granular gas. Phys. Rev. E 59 (1999), p. 1256
15. W. Losert, D. G. W. Cooper, J. Deltour, A. Kudrolli & J. P. Gollub, Velocity statistics in excited granular media. Chaos, 9, 1999, p. 682
16. J. M. Montanero & A. Santos, Computer simulation of uniformly heated granular fluids, to be published in Granular Matter, cond-mat/0002323, (2000)
17. W. Magnus, F. Oberhettinger & R. P. Soni, Formulas and Theorems for the Special Functions of Mathematical Physics. Springer, 1966
18. S. Chapman & T. G. Cowling, The Mathematical Theory of Nonuniform Gases. Cambridge University Press, London, (1960)
19. P. K. Haff, Grain flow as a fluid-mechanical phenomenon. J. Fluid Mech. 134 (1983), p. 401
20. M. P. Allen & D. J. Tildesley, Computer Simulation of Liquids. Clarendon Press, Oxford, (1989)
21. B. D. Lubachevsky, How to simulate billards and similar systems. J. Comp. Phys. 94 (1991), p. 255
22. R. Brito & M. H. Ernst, Extension of Haff's cooling law in granular flows. Europhys. Lett. 43 (1998), p. 497
23. S. Luding, M. Müller & S. McNamara, The validity of "molecular chaos" in granular flows. In World Congress on Particle Technology (Inst. of Chem. Eng., Davis Building, 165-189 Railway Terrace, Rugby CV21 3HQ, UK) (1998), ISBN 0-85295-401-9
24. J. A. G. Orza & R. Brito, (in preparation)
25. S. G. Eubank & J. D. Farmer, Introduction to nonlinear physics. Springer, New York, (1997), p. 106–151
26. S. Luding, M. Huthmann, S. McNamara & A. Zippelius, Homogeneous cooling of rough dissipative particles: theory and simulations. Phys. Rev. E 58 (1998), p. 3416
27. T. Aspelmeier, M. Huthmann & A. Zippelius, Free cooling of particles with rotational degrees of freedom, to be published in Granular Matter, Lecture Notes in Physics. Eds.: T. Pöschel and S. Luding, Springer-Verlag, (2000)
28. O. Herbst, M. Huthmann, & A. Zippelius, Dynamics of inelastically colliding spheres with Coulomb friction: relaxation of translational and rotational energy, to be published in Granular Matter, cond-mat/9911306, (2000)